JACS
JOURNAL OF THE AMERICAN CHEMICAL SOCIETY
Communication
pubs.acs.org/JACS

# Electrocatalytic Oxygen Activation by Carbanion Intermediates of Nitrogen-Doped Graphitic Carbon

Qiqi Li, Benjamin W. Noffke, Yilun Wang, Bruna Menezes, Dennis G. Peters, Krishnan Raghavachari, and Liang-shi Li*

Department of Chemistry, Indiana University, Bloomington, Indiana 47405, United States

Supporting Information

**ABSTRACT:** Nitrogen-doped graphitic carbon has been intensively studied for potential use as an electrocatalyst in fuel cells for the oxygen reduction reaction (ORR). However, the lack of a mechanistic understanding on the carbon catalysis has severely hindered the progress of the catalyst development. Herein we use a well-defined graphene nanostructure as a model system and, for the first time, reveal an oxygen activation mechanism that involves carbanion intermediates in these materials. Our work shows that the overpotential of the electrocatalytic ORR is determined by the generation of the carbanion intermediates, and the current by the rate the intermediates activate oxygen.

The oxygen reduction reaction (ORR) is a crucial step in biological and industrial energy production. In aerobic organisms, the kinetically inert oxygen is activated by enzymes which, by forming complexes with the molecular oxygen,[1,2] either facilitate or bypass the otherwise thermodynamically unfavored superoxide formation.[3,4] To directly convert fuels to electricity in devices such as fuel cells, similar catalysts have been sought after, especially those with high performance, high endurance, and low cost that can outcompete the state-of-the-art ORR electrocatalysts based on Pt or Pt alloys.[5,6] Toward this end, nitrogen-doped graphitic carbon has been intensively studied as a possible candidate.[5] However, mechanistic studies on carbon catalysis are severely hindered by the inhomogeneity and complexity of the catalysts available. Consequently, our understanding has been mainly empirical, and improvements of the catalysts are primarily based on trial and error.[5−7]

Well-defined graphene nanostructures have recently emerged as model systems for studying the carbon catalysis.[8−10] Most of the mesoporous graphitic carbon materials that are of interest for catalytic applications contain curved $sp^2$ domains that have nanometer dimensions.[11] Thus graphene nanostructures, which can be made and functionalized through tightly controlled solution-chemistry synthesis, allow for examination of empirical knowledge on carbon catalysis and enable mechanistic studies that have otherwise been impossible. For instance, Schlögl and co-workers created a phenanthrenequinone cyclotrimer to confirm a previous hypothesis that carbon-catalyzed oxidative dehydrogenation of hydrocarbons is mediated by ketone-like functional groups.[8] We recently used colloidal graphene quantum dots to confirm the covalent interactions between carbon-supported palladium nanoparticles, an important class of catalysts, and their supports.[12] Herein we report on mechanistic studies of the ORR catalyzed by N-doped graphitic carbon with the well-defined graphene nanostructures. We have discovered a mechanism that involves carbanions, for the first time experimentally identifying an intermediate for oxygen activation in these materials. This provides important insights for understanding and possibly improving the ORR activity of N-doped graphitic carbon catalysts.

Recently we reported on electrocatalytic ORR activity of well-defined N-doped graphene nanostructures that resembles the activity of more complex graphitic carbon.[9] This suggests that they may share the same reaction mechanisms and that the nanostructures may be excellent model systems for mechanistic studies of the ORR catalyzed by graphitic carbon in general. In this work we conducted detailed electrochemical studies of such a nanostructure (**1**), aiming to correlate its electronic and redox

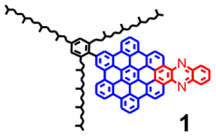

**1**

properties to its catalytic activity. The synthesis of **1** has been reported previously.[9] Besides the conjugated core with a phenazine moiety (marked red), **1** contains a trialkylphenyl group (marked black) to prevent intermolecular $\pi$-stacking and to make **1** soluble in common organic solvents.[10,13] As a result, the properties of **1**, even in the solid state, are primarily determined by the individual molecules rather than their aggregates. Shown in Figure 1 is a cathodic linear sweep voltammetry (LSV) curve obtained with a solid film of 15 $\mu$g of **1** (9.6 nmol) on a glassy carbon electrode in an $O_2$-saturated 0.1 M KOH aqueous solution (pH 13.0, solid curve, left axis). The shoulder near −0.4 V (vs SCE) is attributed to the electrocatalytic reduction of $O_2$.[9] Measurements with a rotating-disk electrode at various rotation speeds indicate that the ORR goes through a four-electron pathway to yield water (Figure S1, Supporting Information (SI)). X-ray photoelectron spectroscopy (XPS) shows that the nitrogen dopants in **1** are "pyridinic" (Figure S2, SI), a form widely present in N-doped carbon with high ORR activity.[5]

We subsequently examined the electrochemical reduction of **1** in the absence of $O_2$, hoping to identify the determining parameters in the catalytic ORR activity. This was achieved

**Received:** December 27, 2013
**Published:** February 17, 2014

ACS Publications © 2014 American Chemical Society



dx.doi.org/10.1021/ja413179n | J. Am. Chem. Soc. 2014, 136, 3358−3361

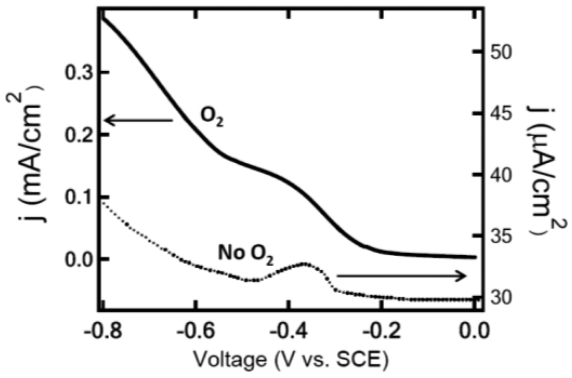


**Figure 1.** Cathodic currents obtained with a solid film of **1** (15 $\mu$g) deposited on a glassy carbon electrode with (solid curve, left axis) and without $O_2$ (dotted curve, right axis) present. The measurements were done in a 0.1 M KOH solution (pH 13.0), the former with LSV and the latter with the DPV technique.

under the same experimental conditions except that the electrolyte solution was saturated with argon. To increase the measurement sensitivity and to eliminate the capacitive background that could conceal any faradaic processes, we applied the differential pulse voltammetry (DPV) technique (details in the SI)[14] and observed a reduction peak (dotted curve in Figure 1, right axis) 2 orders of magnitude smaller than that with $O_2$ present. Remarkably, the reduction of **1** occurs at the same potential as the catalyzed ORR, suggesting that the reduction product(s) of **1** may be responsible for activating the oxygen and initiating the ORR.

To understand the nature of the electrochemical reduction of **1**, we measured the reduction potentials at 25 °C and various pH values and constructed the Pourbaix diagram. As shown in Figure 2a, the reduction of **1** is clearly pH-dependent,

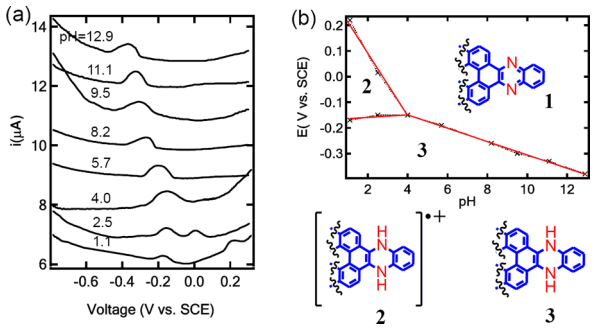


**Figure 2.** pH-dependent electrochemical reduction of **1**. (a) Reduction curves of **1** at various pH values measured with DPV. (b) Poubaix diagram of **1** at 25 °C constructed with the data in (a). The data points are marked with crosses, and the red lines are the best linear fit for the data point. Also shown are the proposed structures for the most stable species in each region of the diagram.

indicating the participation of protons in the process.[15] The Pourbaix diagram obtained is shown in Figure 2b, delineating the potential and pH ranges in which either **1** or its reduction products are thermodynamically stable.[15]

At pH between 1 and 4, **1** undergoes two distinct reduction steps. The potential of the first step varies with pH, following a straight line with a slope of −126 mV per pH unit, consistent with a concerted two-proton, one-electron process.[15] Thus, we conclude that the reduction product is a radical cation with a structure shown in Figure 2b (**2**). The transition from **1** to **2** is described by the following equation,

$$\mathbf{1} + 2H^+ + e^- \rightarrow \mathbf{2}$$

for which the equilibrium potential, according to the Nernst equation, is linear with respect to the pH value with a slope of −118 mV per pH unit at 25 °C.

The second reduction step has a potential that is nearly independent of pH (slope 3 mV per pH unit), indicating an electron-transfer reaction involving no proton. Thus, we determine the product as a neutral dihydrogenated species (**3**, Figure 2b) and the reaction as

$$\mathbf{2} + e^- \rightarrow \mathbf{3}$$

The two potential−pH lines representing the two reduction steps in this pH range intersect at pH near 4. Thus, at higher pH values, **2** is more easily reduced than **1** and undergoes further reduction at the same potential where it is generated. The pH dependence of the electrochemical reduction of **1** and the products are similar to those of phenazine in an aqueous environment,[16] indicating that the N-related functionalities in the graphene nanostructures play an important role in determining the electrochemical processes.

In the pH range between 4 and 13, only one reduction step was observed, as a result of the instability of **2**. Remarkably, the reduction potential now varies with pH, following a straight line with a slope of −27 mV per pH unit, consistent with a concerted one-proton, two-electron process. From stoichiometry we can determine that the product is an amide anion with structure **4** shown in Scheme 1,

$$\mathbf{1} + H^+ + 2e^- \rightarrow \mathbf{4}$$

Because of the delocalization of the negative charge over the conjugated system (some of the resonance structures of **4** shown in Scheme 1), **4** possesses the characters of both an amide anion and a carbanion. Due to its strong basicity, **4** in water will undergo subsequent protonation to yield **3**,

$$\mathbf{4} + H^+ \rightarrow \mathbf{3}$$

involving no electron transfer, and hence is not registered electrochemically. On the basis of the reported p$K_a$ for dihydrophenazine (24.4),[16] we anticipate that the p$K_a$ of **3** should be close to 20, which is confirmed by our DFT calculations (Figure S3, SI).

**Scheme 1. Resonance Structures of 4**

Interestingly, the electrochemical reduction of phenazine in the similar pH range was reported to occur through a concerted two-proton, two-electron process to yield dihydrophenazine in a single step.[16] Our observation that **1** goes through a different pathway is likely due to the large conjugated system stabilizing the anion **4**, so that a two-proton, two-electron path is no longer preferred.[15,17] The size dependence in the reduction kinetics of these conjugated systems will be further investigated in the future.

ORR measurements at various pH values further confirm that the electrochemical reduction of **1** and the ORR catalyzed by it are closely correlated. Figure 3a shows the ORR curves of


dx.doi.org/10.1021/ja413179n | J. Am. Chem. Soc. 2014, 136, 3358−3361

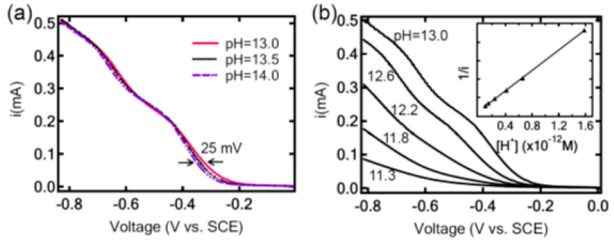


**Figure 3.** pH-dependent ORR activity of **1** in $O_2$-saturated solutions. (a) ORR curves at pH values of 13.0, 13.5, and 14.0. A shift of −25 mV per pH unit is observed in the ORR onset potential, consistent with the shift in the reduction potential of **1**. (b) ORR curves at pH values lower than 13.0, showing the decreasing ORR activity with pH. The inset shows the $1/i \sim [H^+]$ plot obtained from the data at −0.43 V, including some data points at pH values not shown here, and the best fit (solid line). The data point at pH 11.3 was not included in the fitting because of the negligible current. The results were obtained with the LSV technique on a glassy carbon rotating-disk electrode (1500 rpm).

**1** at three pH values, 13.0, 13.5, and 14.0. In this range the curves shift to lower potentials with increasing pH values, whereas the magnitude remains almost the same. The shift is approximately −25 mV per pH unit, consistent with the shift of −27 mV per pH unit in the reduction potential of **1** shown in Figure 2b. It is clear that the ORR onset potential is determined by the reduction of **1**, and thus either **3** or **4** could be responsible for initiating the oxygen reduction.

At lower pH values the ORR activity of **1** quickly decreases, excluding the possibility of **3** activating the oxygen. As shown in Figure 3b, lowering the pH value of the electrolyte solution decreases the ORR activity of **1** drastically, a phenomenon shared by almost all N-doped graphitic carbon except for those containing metals such as Fe or Co.[5,6] When the pH is lowered to 11, almost no catalytic ORR is observed. The residual current at potentials below −0.6 V may be due to uncatalyzed reduction of $O_2$ to the superoxide ($O_2^-$), which has an equilibrium potential of −0.57 V vs SCE.[3] With **3** being the thermodynamically stable species within the whole pH range investigated, we conclude that **3** cannot be responsible for the oxygen activation, and thus the decreasing ORR activity at lower pH values is likely a kinetic effect rather than a thermodynamic one.

The role of the anionic intermediate **4** in activating the molecular oxygen is supported by DFT calculations (*vide infra*). With the M06-2X hybrid density functional,[18] we calculated the affinity of **4** toward triplet oxygen. Figure 4 shows the key portion of the molecular structures corresponding to the lowest calculated Gibbs free energy before and after oxygen activation at a carbon atom next to the protonated nitrogen atom (marked by the "−" sign in the second structure from the left in Scheme 1). The product is essentially an organic peroxide with no net spin, stable by −0.09 eV in vacuum and −0.41 eV in an aqueous environment relative to the reactants. The hydrogen atom attached to the nitrogen migrates to the terminal oxygen, resulting in an O−H···N intramolecular hydrogen bond and the formation of a five-membered ring. The O−O bond length in the adduct is 1.43 Å, significantly longer than that of a triplet oxygen molecule (1.20 Å),[3,4] suggesting that electrons are effectively transferred to the antibonding orbitals of dioxygen. According to our calculations, stable **4**-$O_2$ adducts can also form at other carbon atoms along the edge (Figure S4, SI) to minimize the disruption to the aromatic system. Because the subsequent reduction steps of oxygen after the first electron addition have higher reduction potentials,[3,4] the **4**-$O_2$ adducts will undergo further reduction to yield water as the final product. Therefore, they are likely to be short-lived, and their formation is likely the rate-limiting step for the ORR. In contrast, our calculations confirmed that the covalent binding between **3** and the triplet dioxygen is thermodynamically unfavorable by more than 0.5 eV (Figure S5, SI). In our calculations, the geometries, vibrational frequencies, zero-point energies, and thermal corrections were obtained in vacuum with the M06-2X functional using the 6-31G(d,p) basis set for carbon and hydrogen atoms and 6-31+G(d,p) for nitrogen and oxygen atoms.[19] Aqueous solvation effects were calculated using the SMD solvation model[20] with the 6-31+G(d,p) basis set. The solvation energy was added to a vacuum single-point energy obtained with the larger 6-311+G(2df,p) basis set. All the calculations were conducted with the Gaussian-09 program suite.

**Figure 4.** Geometry around the nitrogen atoms corresponding to the lowest calculated Gibbs free energy before and after oxygen activation by **4**. Oxygen activation occurs at a carbon atom next to the protonated nitrogen atoms. Oxygen, nitrogen, hydrogen, and carbon atoms are marked red, blue, black, and gray, respectively.

To form the **4**-$O_2$ adduct shown in Figure 4, a spin inversion is required, which typically is a slow process without heavy atoms present.[21,22] This restriction in a heterocyclic aromatic system such as **4** is alleviated by the presence of the nitrogen atoms, wherein the mixing of the nonbonding orbitals with the $\pi$-orbitals is well known to enhance the spin−orbit coupling and thus promote the spin inversion.[21,22] Meanwhile, the large conjugated system decreases the exchange interaction between electrons. This effectively decreases the singlet−triplet splitting, and consequently increases the mixing of the states in the singlet and triplet manifolds and can further facilitate the spin inversion.[22,23]

Interestingly, the carbanion mechanism we reveal herein bears remarkable resemblance to the oxygen activation mechanism of flavin, a common cofactor for enzymes that catalyze one- and two-electron-transfer reactions in aerobic metabolism.[2,24] Consisting of a substituted quinoxaline fused with a uracil, the oxidized form of flavin can go through a one-electron reduction to yield a semiquinone, or a two-electron reduction to yield a fully reduced form. The latter, being an anion in biological conditions, is known to activate oxygen by forming a hydroperoxylflavin intermediate.[2,24] In the fully reduced flavin, the anion is stabilized by the electron-deficient uracil moiety, whereas in **1**, it is the large conjugated system that stabilizes the carbanion. In both cases, the nitrogen atoms present in the molecular structures are essential in determining the redox properties and thus the functions of the catalysts.

With the carbanion mechanism, the pH dependence in the ORR activity of **1** arises as a natural result of the competition between oxygen activation by **4** and its protonation that deactivates the catalyst. The observed ORR current is determined by


dx.doi.org/10.1021/ja413179n | J. Am. Chem. Soc. 2014, 136, 3358−3361

$$i = i_0 \frac{R_O}{R_O + R_H}$$

where $R_O$ and $R_H$ represent the rates of **4** reacting with oxygen and with proton, respectively, and $i_0$ the ORR current when $R_H$ is negligible. Figure 3 indicates that the protonation is much faster than oxygen activation at pH 11, and becomes negligible at pH 13, where the current increases little with pH. The oxygen activation rate, obtained from Figure 3a, is on the order of $10^{-2}$–$10^{-1}$ $s^{-1}$ (~$10^{-4}$ A for ~$10^{-8}$ mol of catalyst). Thus, with protonation as a first-order reaction, we estimate its rate constant to be in the range of $10^{10}$–$10^{11}$ $M^{-1}$ $s^{-1}$, consistent with the typical proton-transfer rate constant between water and nitrogen-centered bases.[25] In our estimate here, we used an electron-transfer number of 4 per oxygen molecule, and 12 as the pH value when $R_O$ is comparable to $R_H$. The presence of competition between the two processes is further supported by a linear $1/i \sim [H^+]$ relation obtained experimentally (inset in Figure 3b), consistent with $1/i = 1/i_0\ (1 + R_H/R_O)$.

Our work for the first time experimentally reveals a molecular mechanism for oxygen activation in N-doped graphitic carbon. According to this mechanism, the overpotential of the catalyzed ORR is determined by the generation of the carbanion intermediates, and the current by the rate at which molecular oxygen is activated by the intermediates. This could provide us with valuable insights to improve the ORR catalytic activity of such carbon materials. Parameters that determine whether the ORR follows the four-electron pathway or the two-electron one are not yet clear and are being investigated.

## ■ ASSOCIATED CONTENT

### Supporting Information

Experimental details and extra information on theoretical calculations. This material is available free of charge via the Internet at http://pubs.acs.org.

## ■ AUTHOR INFORMATION


### Corresponding Author

li23@indiana.edu


### Notes

The authors declare no competing financial interest.

## ■ ACKNOWLEDGMENTS

We thank Professors Liming Dai, Srinivasan Iyengar, and Allen Siedle for helpful discussions. This work is supported by the National Science Foundation. The XPS measurement was done at the Nanoscale Characterization Facility of Indiana University.

## ■ REFERENCES


(1) Ho, R. Y. N.; Liebman, J. F.; Valentine, J. S. In *Active Oxygen in Biochemistry*; Valentine, J. S., Foote, C. S., Greenberg, A., Liebman, J. F., Eds.; Chapman & Hall: London, 1995, pp 1–36.

(2) Silverman, R. B. *The Organic Chemistry of Enzyme-Catalyzed Reactions*; Academic Press: London, 2002.

(3) Ho, R. Y. N.; Liebman, J. F.; Valentine, J. S. In *Active Oxygen in Chemistry*, 1st ed.; Foote, C. S., Valentine, J. S., Greenberg, A., Liebman, J. F., Eds.; Chapman & Hall: London, 1996; Vol. 2, pp 1–23.

(4) Sawyer, D. T. *Oxygen Chemistry*; Oxford University Press: New York, 1991.

(5) Yu, D.; Nagelli, E.; Du, F.; Dai, L. *J. Phys. Chem. Lett.* **2012**, *1*, 2165–2173. Wu, G.; Zelenay, P. *Acc. Chem. Res.* **2013**, *46*, 1878–1889.

(6) Yeager, E. *J. Mol. Catal.* **1986**, *38*, 5–25.

(7) Figueiredo, J. L.; Pereira, M. F. R. In *Carbon Materials for Catalysis*; Serp, P., Figueiredo, J. L., Eds.; John Wiley & Sons: New York, 2009; pp 177–217. Boehm, H.-P. In *Carbon Materials for Catalysis*; Serp, P., Figueiredo, J. L., Eds.; John Wiley & Sons: New York, 2009; pp 219–265. Maldonado, S.; Stevenson, K. J. *J. Phys. Chem. B* **2005**, *109*, 4707–4716.

(8) Zhang, J.; Wang, X.; Su, Q.; Zhi, L.; Thomas, A.; Feng, X.; Su, D. S.; Schlögl, R.; Mullen, K. *J. Am. Chem. Soc.* **2009**, *131*, 11296–11297.

(9) Li, Q.; Zhang, S.; Dai, L.; Li, L.-S. *J. Am. Chem. Soc.* **2012**, *134*, 18932–18935.

(10) Yan, X.; Li, B.; Li, L.-S. *Acc. Chem. Res.* **2013**, *46*, 2254–2262.

(11) Radovic, L. R. In *Carbon Materials for Catalysis*; Serp, P., Figueiredo, J. L., Eds.; John Wiley & Sons: New York, 2009; pp 1–44. Harris, P. J. F.; Liu, Z.; Suenaga, K. *J. Phys.: Condensed Mater.* **2008**, *20*, 362201. Hess, W. M.; Herd, C. R. In *Carbon Black: Science and Technology*, 2nd ed.; Donnet, J.-B., Bansal, R. C., Wang, M.-J., Eds.; Marcel Dekker: New York, 1993. Biscoe, J.; Warren, B. E. *J. Appl. Phys.* **1942**, 364–371.

(12) Yan, X.; Li, Q.; Li, L.-S. *J. Am. Chem. Soc.* **2012**, *134*, 16096–16098.

(13) Yan, X.; Li, L.-S. *J. Mater. Chem.* **2011**, *21*, 3295–3300. Yan, X.; Cui, X.; Li, L.-S. *J. Am. Chem. Soc.* **2010**, *132*, 5944–5945.

(14) Osteryoung, J. *Acc. Chem. Res.* **1993**, *26*, 77–83. Bard, A. J.; Faulkner, L. R. *Electrochemical Methods Fundamentals and Applications*, 2nd ed.; Wiley & Sons: New York, 2001.

(15) Weinberg, D. R.; Gagliardi, C. J.; Hull, J. F.; Murphy, C. F.; Kent, C. A.; Westlake, B. C.; Paul, A.; Ess, D. H.; McCafferty, D. G.; Meyer, T. J. *Chem. Rev.* **2012**, *112*, 4016–4093.

(16) Laviron, E.; Roullier, L. *J. Electroanal. Chem.* **1983**, *157*, 7–18.

(17) Hammes-Schiffer, S.; Soudackov, A. V. *J. Phys. Chem. B* **2008**, *112*, 14108–14123.

(18) Zhao, Y.; Truhlar, D. G. *Theor. Chem. Acc.* **2008**, *120*, 215–241.

(19) Ditchfield, R.; Hehre, W. J.; Pople, J. A. *J. Chem. Phys.* **1971**, *54*, 724–728. Hehre, W. J.; Ditchfield, R.; Pople, J. A. *J. Chem. Phys.* **1972**, *56*, 2257–2261. Hariharan, P. C.; Pople, J. A. *Theor. Chem. Acc.* **1973**, *28*, 213–222. Hariharan, P. C.; Pople, J. A. *Mol. Phys.* **1974**, *27*, 209–214. Gordon, M. S. *Chem. Phys. Lett.* **1980**, *76*, 163–168. Francl, M. M.; Pietro, W. J.; Hehre, W. J.; Binkley, J. S.; DeFrees, D. J.; Pople, J. A.; Gordon, M. S. *J. Chem. Phys.* **1982**, *77*, 3654–3665.

(20) Marenich, A. V.; Cramer, C. J.; Truhlar, D. G. *J. Phys. Chem. B* **2009**, *113*, 6378–6396.

(21) Turro, N. J. *Modern Molecular Photochemistry*; University Science Books: Sausalito, CA, 1991.

(22) Lower, S. K.; El-Sayed, M. A. *Chem. Rev.* **1966**, *66*, 199–241.

(23) Mueller, M. L.; Yan, X.; McGuire, J. A.; Li, L.-S. *Nano Lett.* **2010**, *10*, 2679–2682. McClure, D. S. *J. Chem. Phys.* **1952**, *20*, 682–686.

(24) Ghisla, S.; Massey, V. *Eur. J. Biochem.* **1989**, *181*, 1–17. Palfey, B. A.; Ballou, D. P.; Massey, V. In *Active Oxygen in Biochemistry*; Valentine, J. S., Foote, C. S., Greenberg, A., Liebman, J. F., Eds.; Chapman & Hall: London, 1995; pp 37–83. Bruice, T. C. *Acc. Chem. Res.* **1980**, *13*, 256–262. Muller, F. *Top. Curr. Chem.* **1983**, *108*, 71–107. Massey, V. *J. Biol. Chem.* **1994**, *269*, 22459–22462.

(25) Eigen, M. *Angew. Chem.* **1964**, *3*, 1–19.